Persistent Replication of Severe Acute Respiratory Syndrome Coronavirus in Human Tubular Kidney Cells Selects for Adaptive Mutations in the Membrane Protein[▽]

Filippo Pacciarini,[1]† Silvia Ghezzi,[1]† Filippo Canducci,[2,6] Amy Sims,[3] Michela Sampaolo,[2,6]
Elena Ferioli,[5] Massimo Clementi,[2,6] Guido Poli,[4,6] Pier Giulio Conaldi,[7]
Ralph Baric,[3] and Elisa Vicenzi[1]*

*Viral Pathogens and Biosafety Unit, San Raffaele Scientific Institute, Milano, Italy[1]; Laboratory of Microbiology and Virology,
San Raffaele Scientific Institute, Milano, Italy[2]; University of North Carolina at Chapel Hill, Chapel Hill, North Carolina[3];
AIDS Immunopathogenesis Unit, San Raffaele Scientific Institute, Milano, Italy[4]; Department of Medicine and
Public Health, University of Insubria, Varese, Italy[5]; Vita-Salute San Raffaele University, School of
Medicine, Milano, Italy[6]; and Laboratory of Clinical Pathology, Microbiology and Virology,
Mediterranean Institute for Transplantation and Advanced Specialised Therapies,
University of Pittsburgh Medical Center—Italy, Palermo, Italy[7]*

Severe acute respiratory syndrome (SARS) is a systemic disease characterized by both lung pathology and widespread extrapulmonary virus dissemination causing multiple organ injuries. In this regard, renal dysfunction is an ominous sign in patients with SARS. Indeed, clusters of SARS coronavirus (SARS-CoV) particles have been detected in the cytoplasm of renal tubular epithelial cells in postmortem studies, explaining the presence of infectious virus in the urine of SARS patients. In order to investigate the potential SARS-CoV kidney tropism, we have evaluated the susceptibility of human renal cells of tubular and glomerular origin to in vitro SARS-CoV infection. Immortalized cultures of differentiated proximal tubular epithelial cells (PTEC), glomerular mesangial cells (MC), and glomerular epithelial cells (podocytes) were found to express the SARS-CoV receptor angiotensin-converting enzyme 2 on their surface. Productive infection, however, occurred only in PTEC but not in glomerular cells. A transient infection with poor virus production was observed in MC, whereas podocytes were not permissive to SARS-CoV infection. In contrast to the cytopathic infection of the Vero E6 cell line, SARS-CoV did not cause overt cytopathic effects in PTEC or MC. Of interest, PTEC, but not MC, maintained stable levels of SARS-CoV production in serial subcultures, suggesting a persistent state of infection. In this regard, a SARS-CoV variant with increased replication capacity in PTEC was selected after four serial subculture passages. This SARS-CoV variant acquired a single nonconservative amino acid change from glutamic acid (E) to alanine (A) at position 11 in the viral membrane (M) protein. The E11A point mutation was sufficient for enhanced SARS-CoV replication and persistence in PTEC when introduced in a SARS-CoV recombinant infectious clone. These findings indicate that human PTEC may represent a site of SARS-CoV productive and persistent replication favoring the emergence of viral variants with increased replication capacity, at least in these kidney cells.

The severe acute respiratory syndrome (SARS) emerged in China and spread to several countries worldwide in a few months, resulting in the infection of 8,096 people and 774 deaths from 2002 to 2003 (52). A novel human coronavirus (SARS-CoV) was independently isolated from SARS patients on three different continents (12, 27, 28, 38). Human-to-human SARS-CoV transmission was contained in the same year; however, animal-to-human transmission has been documented, implying that the virus could reemerge as a human pathogen. Indeed, the full eradication of SARS-CoV might be extremely difficult since its natural host seems to be a wild rather than a domestic animal (19, 32).

The main target organs of SARS-CoV are the lungs, which can be severely damaged by the infection, causing acute respiratory distress syndrome, which is frequently fatal (39). Several reports, however, have highlighted that SARS patients often showed evidence of lymphoid tissue, liver, and kidney dysfunctions (13, 16, 49). In particular, a small proportion (6.7%) of SARS patients suffered acute renal impairment; interestingly, the involvement of the kidney in SARS cases has been associated with a high (91.7%) mortality rate (5). Immunohistochemistry, in situ hybridization, and electron microscopy examination of autopsy samples obtained from these patients revealed SARS-CoV virions, RNA, and/or antigen in lung and in a number of other organs, including the kidneys (16). These observations indicate that SARS-CoV causes a systemic infection with widespread extrapulmonary dissemination with viral shedding not only in respiratory secretions, but also in stool and urine (23, 54).

This broad dissemination of SARS-CoV infection has been correlated, in part, to the multiple-organ expression of angiotensin-converting enzyme 2 (ACE2), which serves as the cell surface SARS-CoV receptor (21, 31), and to a lesser extent coreceptors such as liver-specific *I*CAM-*g*rabbing *n*on-integrin (L-SIGN) (24). ACE2 is expressed by type 1 and 2 pneumocytes, enterocytes of the small intestine, and at the brush bor-

der of the proximal tubular epithelial cells (PTEC) of the kidney (17). In this regard, it is interesting to note that the Vero cell line, which was crucial in the successful isolation of SARS-CoV from nasopharyngeal material of infected patients, was derived from the kidney of an African green monkey (12, 14, 44, 51). In addition, cell lines of human kidney origin have shown susceptibility to SARS-CoV infection and, among these, the human embryonic kidney 293 cells support SARS-CoV productive infection (56).

The goal of our study was to investigate the susceptibility of the main cell types present in the nephron in order to characterize a potential tropism of SARS-CoV infection in the kidney. In this regard, glomerular mesangial cells (MC) are specialized pericytes of vascular smooth muscle origin exerting several physiological functions, such as the control of glomerular hemodynamics, clearance of macromolecules, and immune complexes, whereas epithelial cells (podocytes) play an essential role in glomerular perm-selectivity (1, 25). Finally, PTEC are responsible for the readsorption of about 60% of the glomerular ultrafiltrate (34).

In the present study, immortalized human PTEC, MC, and podocytes derived from glomerular and cortical tubules were selected as in vitro models to test their susceptibility to SARS-CoV infection. Unexpectedly, SARS-CoV productive and persistent infection was only supported by PTEC and was associated with the emergence of a single-amino-acid mutation in the membrane (M) protein.

MATERIALS AND METHODS

Cells. The Vero E6 cell line was obtained from the Istituto Zooprofilattico of Brescia, Italy, and was maintained in Eagle's minimum essential medium (EMEM; Cambrex Bio Science, Verviers, Belgium) supplemented with 10% fetal bovine serum (FBS) and penicillin-streptomycin (complete medium). The immortalized human PTEC line was previously characterized (42). Differentiated glomerular cell lines were obtained by immortalization through the infection with an adenovirus 5-simian virus 40 hybrid of pure primary cultures established as described previously (6). Individual foci of immortalized cells were subcultured and characterized on the basis of cell morphology, functional tests, and the expression of cell-specific antigens, according to established criteria (48). MC and podocyte lines were selected and used between passages 25 and 45, as reported previously (7–9). PTEC were maintained in RPMI 1640 (Cambrex Bio Science) supplemented with 10% FBS, whereas MC was maintained in RPMI 1640 plus 20% FBS. Podocytes were cultivated in Dulbecco's MEM (DMEM, Cambrex Bio Science) supplemented with 20% FBS.

Virus. The SARS-CoV HSR1 strain was isolated from a sputum sample of an Italian male who traveled in 2003 in Asia and returned to Italy affected by SARS. The sputum was collected at the peak of illness and stored at -80°C for 3 weeks prior to virus isolation on Vero cells. Primary, secondary, and tertiary viral stocks were generated in Vero cells as previously described (51). In order to measure the virus titer present in the viral stocks, a plaque assay was optimized in Vero E6 cells (40). Briefly, confluent Vero E6 cells (1.5×10^6 cells) seeded in six-well plates (Falcon, Becton Dickinson Labware, Lincoln Park, NJ) were incubated in duplicate with 1 ml of phosphate-buffered saline (PBS) containing 100 µl of SARS-CoV in 10-fold serial dilutions. After 1 h of incubation, the viral inoculum was removed and 1 ml of carboxymethylcellulose (Sigma Chemical Corp., St. Louis, MO) with DMEM supplemented with 1% FBS was overlaid on each well. After 6 days of incubation, the cells were stained with 1% crystal violet (Sigma) in 70% methanol. The plaques were counted after examination with a stereoscopic microscope (SMZ-1500; Nikon Instruments, Firenze, Italy) and the virus titer was calculated in PFU/ml. The entire SARS-CoV HSR1 genome sequence is deposited in the GenBank database under accession no. AY323977.

Infections. Vero E6 cells, PTEC, MC, and podocytes (4×10^6 cells/flask in 10 ml) were seeded in 25-cm² tissue culture flasks (Falcon) and incubated for 24 h. Cells at 70 to 80% confluence were washed twice with PBS and inoculated with 500 µl of virus suspension (tertiary stock HSR1-III) corresponding to 4×10^5 PFU per flask and to a multiplicity of infection (MOI) of 0.1. Inoculated cell

cultures were incubated at 37°C for 1 h before being washed five times with EMEM and incubated for 96 h in complete medium. A mock infection was performed in parallel for each cell line. The cell monolayers were examined daily for cytopathic effects (CPE). Aliquots of culture supernatants were also collected daily and stored at -80°C; the cells were trypsinized and spun to obtain a cell pellet. The remaining cultures were trypsinized 3 days postinfection (p.i.) and diluted 1:2 in fresh complete medium. This procedure was serially repeated every 3 days up to four consecutive times. During each passage, supernatants and cell pellets were harvested every 24 h and stored at -80°C. The virus titer present in the supernatant of each passage was determined by open reading frame 1b (ORF-1b) real-time PCR and by a plaque infectivity assay in Vero E6 cells as described previously (51). To determine the ability of SARS-CoV present in the first and last supernatants to reinfect either PTEC or Vero E6 cells, 1.5×10^6 cells were seeded in six-well plates (Falcon) and, 24 h later, they were inoculated with MOIs of 0.03 and 0.006, respectively. Cell cultures were incubated at 37°C for 1 h and then washed five times with EMEM and incubated for 96 h in complete medium. The kinetics of viral replication were determined by quantification of ORF-1b in aliquots of the supernatants collected daily up to 7 days.

ACE2 cell surface expression. Renal epithelial cells (2×10^5) were detached with Accutase (Uptima Interchim, Montluçon, France) and washed with PBS containing 2% FBS. One microgram of a polyclonal antibody (Ab) against human ACE2 (R&D Systems, Minneapolis, MN) was applied to 2×10^5 cells for 30 min at 4°C. After 2 washes with PBS containing 2% FBS, cells were exposed to 1 µg of swine anti-goat phycoerythrin-conjugated Ab (G50001; Caltag Laboratories, Burlingame, CA) for 30 min at 4°C. The cells were washed twice with PBS containing 2% FBS and 0.1% Na-azide, fixed in 2% formaldehyde–PBS, and subjected to flow cytometry using a FACScan flow cytometer (Becton Dickinson, Franklin Lakes, NJ), and the results were analyzed by the CellQuest program (Becton Dickinson).

Real-time RT-PCR mRNA analysis. Total RNA was isolated by the TRIzol method (Invitrogen, Carlsbad, CA). cDNA was synthesized from 2 µg of total RNA using Superscript II reverse transcriptase (RT) (Invitrogen) with random primers. A real-time PCR that amplifies a 141-bp fragment specific for the transcript of the nucleocapsid protein was used to detect and quantify SARS-CoV in the infected cells. The assay used ABI-7700 Prism instrumentation (Applied Biosystems, Foster City, CA), with primers and probe designed with the associated Primer Express software. The following primer pair and probe were added to the universal PCR master mix (Applied Biosystems) at 200 and 100 nM, respectively, in a final volume of 25 µl: forward primer, 5′-AACCAACCTCGA TCTCTTGTAGATCT-3′; reverse primer, 5′-TCCATTCTGGTTATTGTCAG TTGAA-3′; and probe, 6-carboxyfluorescein–TCTCTAAACGAACAAATTA AAATGTCTGATAATGGAC–6-carboxytetramethylrhodamine. The cycling conditions were as follows: 2 min at 50°C, 10 min at 95°C, and then 40 cycles of 15 s at 95°C and 1 min at 60°C. The standard was obtained by cloning the 141-bp fragment into the pCR2.1 plasmid using the TA cloning kit (Invitrogen). A linear distribution ($r = 0.99$) was obtained between 10^1 to 10^8 copies. To correct for intersample variations in RT-PCR efficiency and errors in sample quantification, a set of 18S PCRs was performed as an invariant endogenous control in the assay. Primer pair and probe for 18S were obtained from Applied Biosystems and used according to the manufacturer's directions.

Viral RNA was purified from 140 µl of the cell supernatant using the viral RNA Mini kit (Qiagen). Full-length genomic RNA was retrotranscribed by using Superscript II RT (Invitrogen) with random primers. Briefly, the real-time PCR of a 77-bp fragment of ORF-1b was obtained by using the following primer pair and probe, added to the universal PCR master mix (Applied Biosystems) at 200 nM in a final volume of 25 µl: primer BNITMSARS1, 5′-TTATCACCCGCGA AGAAGCT-3′; primer BNITMSARAS2, 5′-CTCTAGTTGCATGACAGCCCT C3′; and probe BNITMSARS, 6-carboxyfluorescein-TCGTGCGTGGATTGGC TTTGATGT-6-carboxytetramethylrhodamine (40). The standard was obtained by cloning the 77-bp fragment into the pCR2.1 plasmid using the TA cloning kit (Invitrogen). A linear distribution ($r = 0.99$) was obtained between 10^1 and 10^8 copies.

Sequencing of the SARS-CoV HSR1 genome released by infected PTEC. After reverse transcription, amplification of virus genome sequences was carried out with 68 partially overlapping primers encompassing the whole viral genome by using *Pfu* TURBO DNA polymerase (Stratagene, La Jolla, CA). Each 750-bp fragment was gel isolated by means of a QIAQuick gel extraction kit (Qiagen) and directly sequenced from both directions inward and outward. SeqScape version 2.0 (Applied Biosystems) software was used for base identification, editing, and assembly of the fragments. The cDNA of the M coding sequence was amplified by the primer pair MF (CCTGATCTTCTGGTCTAAACG) and MR (CTCTGCTATTGTAACCTGGAAGTC) with the *Pfu* TURBO DNA polymerase (Stratagene). The PCR products were gel purified by means of a QIAQuick
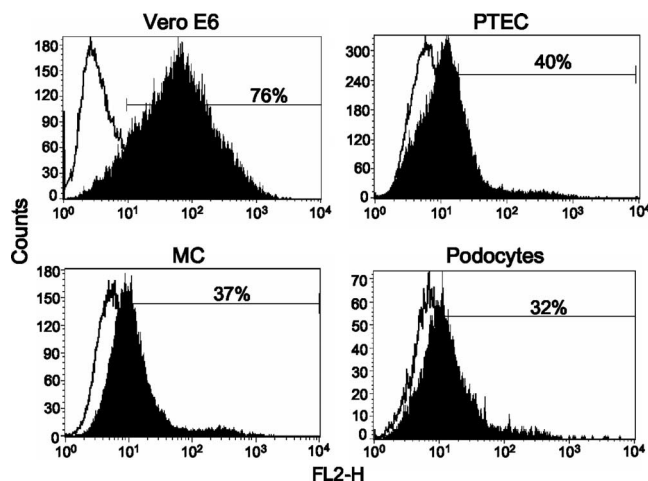
FIG. 1. ACE2 expression in kidney cell lines. Kidney cell lines derived from African green monkeys (Vero E6), human kidney PTEC, MC, and podocytes were analyzed for ACE2 expression by labeling the cell surface with an anti-ACE2 polyclonal Ab. The full histograms indicate cells testing positive for ACE2 expression, whereas the open histograms represent the staining with a control Ab (swine anti-goat phycoerythrin-conjugated secondary Ab). The number on the upper right indicates the percentage of ACE2$^+$ cells.
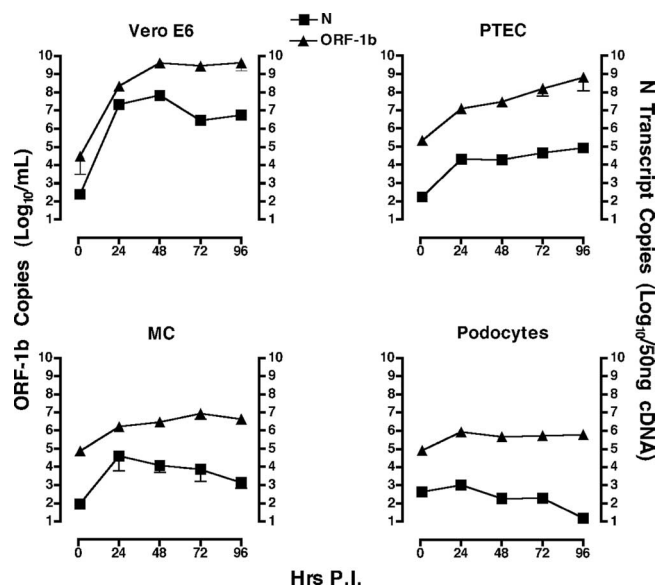

FIG. 2. Kinetics of SARS-CoV replication in kidney cells. Vero E6 cells, PTEC, MC, and podocytes were infected with SARS-CoV HSR1 at an MOI of 0.1. Virus replication was measured by real-time PCR of the full genome (▲) in the supernatant of infected cells harvested every 24 h up to 4 days p.i. The quantification of subgenomic transcripts was carried out by real-time PCR on retrotranscribed cDNA obtained from infected cells every 24 h up to 4 days p.i. The nucleocapsid (N) $\log_{10}$ copy number (■) was normalized by 50 ng of 18S RNA measured by real-time PCR. Values represent the mean number of ORF-1b copies ± standard deviation expressed as $\log_{10}$/ml obtained in three independent experiments.

gel extraction kit (Qiagen) and cloned into pZERO vector (Invitrogen). Individual colonies were inoculated, and after plasmid extraction, sequences of individual clones were obtained with M13+ and M13− primers by an automatic sequencer (ABI Prism 3100; Applied Biosystems).

Insertion of mutations in an infectious clone of SARS-CoV. Two nucleotide changes, G26425A and A26429C, causing E>K and E>A amino acid mutations, respectively, were inserted by site-directed mutagenesis into cDNA clones and used to construct and rescue an infectious clone obtained from the recombinant Urbani SARS-CoV strain (GenBank accession no. AY278741), as described previously (57). In brief, the mutated F fragment and wild-type (WT) fragments A through E were amplified in *Escherichia coli*, isolated by restriction digestion, and separated on agarose gels. The fragments were then gel extracted and ligated together to generate a genome-length cDNA. Full-length genomic transcripts were generated using mMessage mMachine kits from Ambion, which were transfected directly into Vero E6 cells. Cells were seeded and monitored for evidence of CPE, while the supernatants were harvested and passaged as described above.

For the mutations at nucleotide positions 26425 and 26429, respectively, primer pairs 5′-CAACGGTACTATTACCGTTAAGGAGCTTAAACAACTC CTG-3′ and 5′-CAGGAGTTGTTTAAGCTCCTTAACGGTAATAGTACCG TTG-3′ and 5′-CGGTACTATTACCGTTGAGGCGCTTAAACAACTCCTG GA-3′ and 5′-TCCAGGAGTTGTTTAAGCGCCTCAACGGTAATAGTACC G-3′ were used.

The infectious and all recombinant viruses produced in this study were isolated, sequenced, confirmed, and propagated on Vero E6 cells in DMEM containing 10% fetal clone II, 10% tryptose phosphate broth, and 1× gentamicin-kanamycin.

RESULTS

Susceptibility of human kidney cell lines to SARS-CoV infection. It is well established that the susceptibility of cell lines derived from different organs and tissues to SARS-CoV infection is strongly influenced by their level of expression of the virus receptor ACE2 (31, 33, 41). Thus, in order to determine the capacity of SARS-CoV to infect human cells from different components of the renal corpuscle, ACE2 surface expression was determined by anti-ACE2 polyclonal Ab staining and FACS analysis of PTEC, MC, and podocytes in comparison to Vero E6 cells. The expression of ACE2 was highest in Vero E6

cells in comparison to all human kidney-derived cell lines; small differences of expression were noted among the latter with the gradient PTEC > MC > podocytes (Fig. 1).

A key feature of CoVs is their unique transcription strategy that leads to the synthesis of a nested set of 3′-coterminal subgenomic mRNAs, encoding structural and accessory proteins (45). The synthesis of each subgenomic mRNA involves a discontinuous step by which the body transcription regulatory sequence is fused to the genomic 5′ leader sequence. The fusion of 5′ leader and 3′ body transcription regulatory sequences during discontinuous transcription corresponds to the individual transcription units (45, 47). By sequencing the junction between the leader sequence and the nucleocapsid gene of SARS-CoV HSR1 obtained from Vero E6-infected cells, a primer pair and probe specific for the detection of the subgenomic nucleocapsid RNA were designed. The replication kinetics of SARS-CoV in Vero E6 and kidney cell lines are shown in Fig. 2, as measured by real-time PCR assay for nucleocapsid transcripts in infected cells and for ORF-1b viral genomes in the supernatant. The peak of viral replication was reached 48 h p.i. in Vero E6 cells (Fig. 2). Similar to Vero E6 cells, a titer increase of 5 $\log_{10}$/ml above the input virus was achieved in PTEC 96 h p.i.; the levels of intracellular nucleocapsid transcripts were, however, approximately 1,000-fold lower in PTEC than in Vero E6 cells. Although the levels of SARS-CoV HSR1 nucleocapsid transcripts in MC were 2 $\log_{10}$ above the input virus detectable 24 h p.i., they were significantly lower than those observed in PTEC. In contrast, the
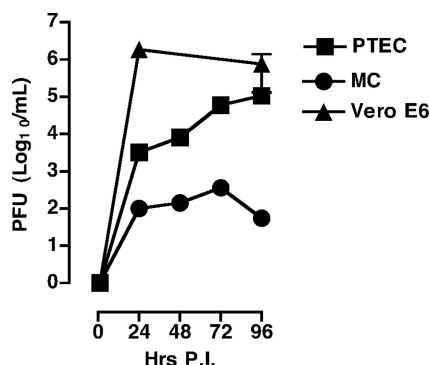
FIG. 3. Kinetics of SARS-CoV growth. The supernatants from infected PTEC (■), MC (●), and Vero E6 (▲) cells, harvested every 24 h up to 4 days p.i., were tested in a Vero E6 plaque assay to determine the levels of infectious virus. Values represent the mean PFU ± standard deviation, expressed as $\log_{10}$/ml obtained in three independent experiments.

FIG. 4. Cell viability after SARS-CoV HSR1 infection of Vero E6 and human kidney cells. Cells were exposed to 4×10^5 PFU of SARS-CoV HSR1 and stained with Trypan blue dye after 72 h p.i. Photographs were taken using a digital camera connected to the light microscope at a magnification of ×40. CPE (dark) was evident in Vero E6 cells, whereas SARS-CoV-infected human kidney epithelial cells did not show decreased viability in comparison to uninfected control cell cultures.

nucleocapsid transcripts did not increase in virus-exposed podocytes over the background levels (Fig. 2).

In order to correlate the copy number of ORF-1b obtained by real-time PCR with the number of infectious virions, a plaque assay was performed in Vero E6 cells with the supernatants obtained from infected human kidney cells and Vero E6 cells as a control. The kinetics of infectious virus production showed that titers of 1.07×10^5 and 1.34×10^6 PFU/ml were obtained 96 h p.i. in PTEC and Vero E6 cells, respectively, whereas the maximum yield of infectious virus in MC culture supernatants was 3.6×10^2 PFU/ml 72 h postinfection (Fig. 3). These results support a direct correlation between the number of the viral genomes and the infectious virus titers released by infected cells (Fig. 2 and 3, respectively) confirming previous observations that approximately 2 to 3 $\log_{10}$ of SARS-CoV genomes are required to form a single plaque in Vero E6 cells (40, 51).

A cytopathic effect (CPE) appeared as early as 48 h after virus inoculation in Vero E6 quickly spreading to the entire cell monolayer by 72 h (Fig. 4). In contrast, PTEC and MC viability was only slightly affected by virus replication, as demonstrated by Trypan blue dye exclusion and lack of evidence of a SARS-CoV-induced CPE (Fig. 4). The percentage of viable PTEC and MC ranged constantly between 80 and 90%, in spite of the different levels of virus replication (that were higher in PTEC than in MC; Fig. 2 and 3). We cannot exclude that the lack of evidence of a CPE in PTEC might in part be dependent on both slower kinetics and lower efficiency of viral replication in PTEC compared to Vero E6 cells.

SARS-CoV causes a persistent infection of PTEC but not MC. Since the infection of PTEC and MC cultures with SARS-CoV did not result in a clear CPE, we investigated the possibility that SARS-CoV might establish a persistent infection in these cells, as previously observed in the colonic epithelial LoVo cell line, in which SARS-CoV replicates with no evidence of CPE (2) and in Vero E6 cells after the acute lytic phase of replication (36, 55). For this purpose, infected PTEC and MC cultures were regularly split every 3 days up to four passages. The supernatants were collected prior to each cell subcultivation and tested for the presence of ORF-1b by real-
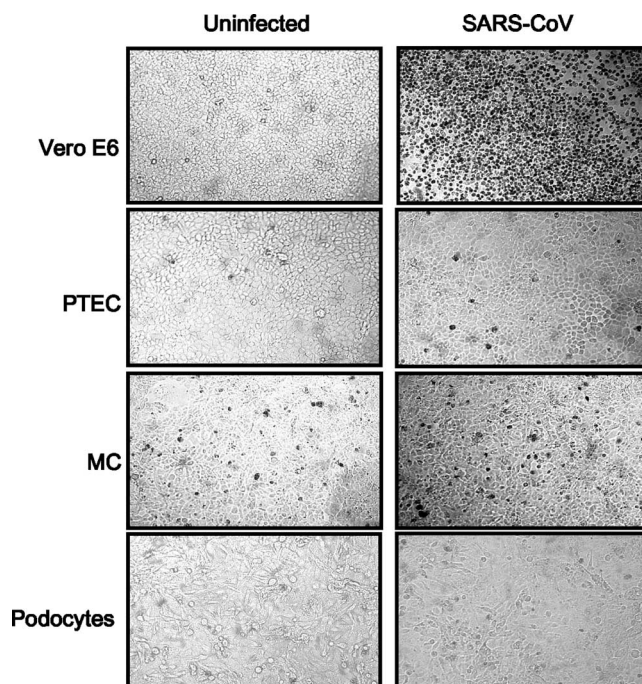
time PCR: time zero hours (T_0) defined the supernatant harvested prior to the first subcultivation, and the following collections were indicated by serial numbers up to four cell subcultivations in five independent experiments. Continuous production of SARS-CoV was maintained in PTEC within the range of 7.44 to 8.27 $\log_{10}$ copies/ml in the absence of evident CPE in three out of five independent experiments (Fig. 5). In contrast, the viral copy number in the supernatants of MC decreased from 5 to approximately 2 $\log_{10}$ copies/ml after four serial cell divisions. The infectious virus titers in T_0 and T_4 PTEC supernatants were 3.3×10^4 and 4.2×10^4 PFU/ml, respectively, as tested in Vero E6 cells.

Evolution of SARS-CoV in persistently infected PTEC. In order to evaluate whether viral mutations evolved during the persistent infection of human PTEC, sequencing of the entire SARS-CoV genome was carried out on genomic RNA extracted from T_4 supernatant. The alignment of SARS-CoV sequences obtained from the T_4 supernatant with the reference HSR1 strain (GenBank accession no. AY323977) revealed the substitution of only 1 nucleotide out of 29,751 mapping in the coding sequence of the M protein at position 26429 and resulting in a mutation of glutamic acid (E) into alanine (A) at position 11.

In order to better characterize the kinetics of the emergence of viruses carrying this mutation, the M coding sequence was amplified from SARS-CoV present in the supernatant collected prior to each cell subcultivation. By cloning and sequencing an average of 10 independent clones from T_0 to T_4,
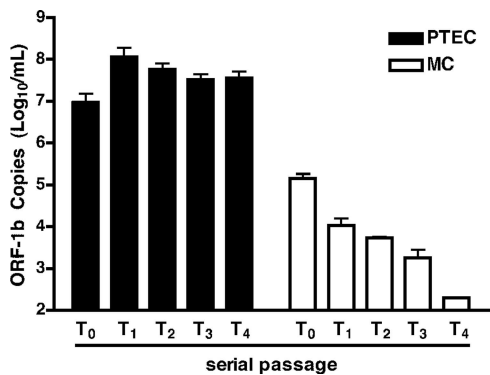
FIG. 5. Persistent virus production in PTEC but not in MC. Cells were infected with SARS-CoV HSR1 at an MOI of 0.1. After 3 days, cultures were split and this procedure was repeated every 3 days up to four passages. Cultivation passages are indicated with a T, and the number in subscript indicates the serial passage. At each passage, 50% of the cells were seeded in fresh medium. The SARS-CoV copy number was calculated by real-time PCR of ORF-1b in cell supernatants collected prior to cell subculture. Values represent the mean number of ORF-1b copies ± standard deviation expressed as log_{10}/ml obtained in three independent experiments.

FIG. 7. Kinetics of SARS-CoV HSR1 replication in PTEC and Vero E6 cells infected with the supernatant obtained from the T_0 culture prior to cell division and the T_4 subculture. PTEC and Vero E6 cells were infected at MOIs of 0.03 and 0.006, respectively. Both PTEC and Vero E6 cells were also incubated with a 1:1 mixture of T_0 and T_4 supernatants containing 5×10^4 PFU/each. Replication kinetics were measured by real-time PCR of ORF-1b in the supernatant harvested every 24 to 48 h p.i. Values represent the mean number of ORF-1b copies ± standard deviation expressed as log_{10}/ml obtained in three independent experiments.

we observed that the E11A mutation firstly appeared in the T_3 supernatant in 2 out of 10 clones and became dominant (in 10 out 10 clones) in T_4 (Fig. 6). The viral stock HSR1-III was characterized by a mixture in which one variant had a G→A change at position 26425 leading to amino acid change E10K. This variant was selected during the serial subcultivation and disappeared with the emerging E11A mutation. These results suggest that the E11A mutation is selected as consequence of virus adaptation to replicate in PTEC cells.

Analysis of SARS-CoV M mutant replication in PTEC. In order to test whether the emergence of E11A mutation was consequent to SARS-CoV adaptation in PTEC, the initial (T_0) and the last (T_4) supernatants from one of the three experiments reported in Fig. 5 were further analyzed. The virus titer was determined in these supernatants by either plaque assay on Vero E6 cells or ORF-1b real-time PCR (40, 51). T_0 and T_4 supernatants contained 3.3×10^4 and 4.2×10^4 PFU/ml and 3.7×10^7 and 7.6×10^7 ORF-1b copies/ml, respectively. In order to evaluate differences in replication efficiency in T_0 and T_4 supernatants, cultures of PTEC were infected at the MOI of 0.03, lower than the MOI of 0.1 used in the experiments shown in Fig. 2. In addition, PTEC were incubated with a 1:1 mixture
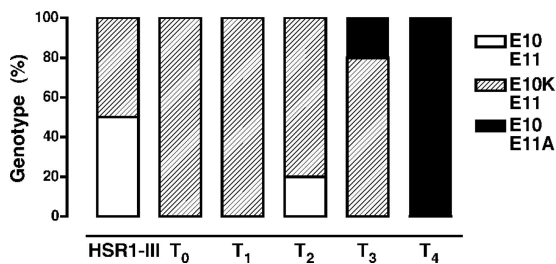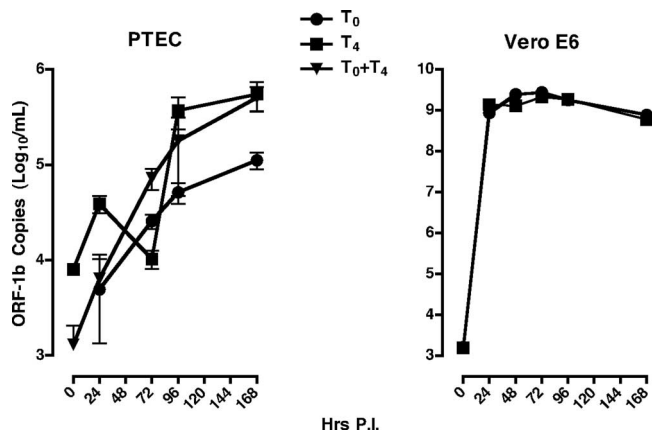
FIG. 6. Proportion of viral quasispecies in the M protein following serial subculturing of PTEC. The percentage is relative to 10 clones obtained from SARS-CoV HSR1-III passaged three times in Vero E6 cells and each time point from T_0 to T_4.

of T_0 and T_4 supernatants containing 5×10^4 PFU/each in order to reveal a potential interference between virus variants generated during PTEC persistent infection. Cultures incubated with the HSR1-III virus were maintained in parallel as a control. The kinetics of SARS-CoV replication, as measured by ORF-1b real-time PCR of T_0, T_4, and the $T_0 + T_4$ mixture, are shown in Fig. 7. The T_4 virus showed a replication capacity higher than the T_0 virus in terms of both kinetics and levels of ORF-1b expression, whereas PTEC infected with a $T_0 + T_4$ mixture showed intermediate kinetics, but, ultimately, the levels of virus replication were comparable to those of the T_4 virus (Fig. 7, left panel). In contrast, the levels of ORF-1b copies present in the supernatant of Vero E6 cells infected with either T_0 or T_4 viruses were superimposable (Fig. 7, right panel). This finding suggests that a superior replicative capacity in PTEC is conferred by the E11A mutation in the M glycoprotein.

Replication kinetics of SARS-CoV infectious clone containing mutations in the M protein. The contribution of the M protein E10K and E11A mutations to virus replication in PTEC and Vero E6 cells was further investigated in the context of the recombinant viruses derived from an infectious clone obtained from SARS-CoV Urbani (57). The kinetics of viral replication of WT and isogenic recombinant viruses encoding the E11A or E10K mutations are shown in Fig. 8. The E11A mutant virus replicated more efficiently than WT virus in PTEC, whereas E10K mutant virus showed replication kinetics similar to those of WT virus (Fig. 8A). The replication kinetics of the three viruses were indistinguishable in Vero E6 cells when cells were infected with WT and mutant viruses at the MOI of 0.00006; nonetheless, the levels of ORF-1b transcripts 24 h p.i. were approximately 1 log_{10} superior in Vero E6 cells infected with the E11A mutant to those from cells infected with WT virus (Fig. 8B). The replicative advantage of the E11A mutation for replication in PTEC was further confirmed by plaque assay in Vero E6 cells in supernatants harvested at
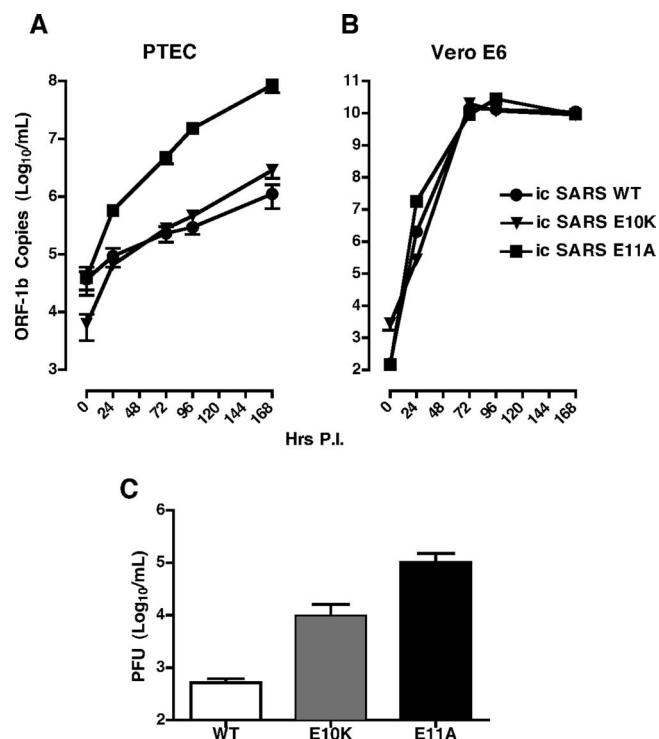
FIG. 8. Kinetics of viral replication of WT and mutant infectious clone (ic) in PTEC (A) and Vero E6 cells (B). Replication kinetics were measured by real-time PCR of ORF-1b in the supernatant harvested every 24 to 48 h p.i. Values represent the mean number of ORF-1b copies $\pm$ standard deviation expressed as $\log_{10}$/ml obtained in two independent experiments. Infectious virus present in the PTEC supernatant 168 h p.i. (C) was determined in a Vero E6 plaque assay. Values represent the mean PFU $\pm$ standard deviation as $\log_{10}$/ml.

168 h p.i. (Fig. 8C). These results confirmed that the E11A mutation is advantageous for SARS-CoV replication.

DISCUSSION

In this study, we have shown that differentiated human renal tubular epithelial cells (PTEC) and, to a lesser extent, glomerular MC supported productive in vitro infection of SARS-CoV. In contrast, glomerular epithelial cells (podocytes) did not support productive SARS-CoV replication in spite of expression of ACE2 on their surface. Unlike Vero E6 cells, PTEC and MC showed no evidence of CPE or reduced cell proliferation upon infection by SARS-CoV. Interestingly, SARS-CoV replicated in MC only transiently, whereas a persistent state of infection characterized by a stable release of infectious virus was observed in PTEC. This productive infection profile in PTEC was associated with the emergence of a viral variant characterized by a single-amino-acid substitution (E11A) in the M protein showing a replicative advantage versus WT in PTEC. This observation was confirmed by the replication kinetics of virus derived from an infectious molecular clone in which the E11A was introduced.

The renal cell lines used in this study maintain phenotypic and functional features identical to those of the tubular and glomerular cells in tissue, and for these reasons, they have been used as models to investigate the interaction between different

viruses and human renal cells (6, 7, 9). For example, human immunodeficiency virus type 1 was shown to induce distinct pathogenic effects in glomerular and tubular cells, mimicking the pathological features of HIV-associated nephropathy in vivo (7, 8). Our in vitro findings support the evidence of kidney involvement in the natural history of SARS-CoV infection, providing an experimental model for the virus tropism to the kidney having potentially relevant implications for SARS pathogenesis (5, 11, 13, 16). In this regard, extrapulmonary dissemination of the virus into all major organs, including the distal renal tubules, has been confirmed in several patients by electron microscopy, in situ hybridization, and real-time PCR (16, 29). Our results demonstrate that the tubular epithelial cells are indeed susceptible to SARS-CoV infection and replication in vitro. The establishment of productive viral replication in these cells with release of infectious progeny is in agreement with the presence of virus in the urine, as detected in SARS patients (20, 37). Since viruses are much larger than filterable micromolecules, patient's viruria is likely a consequence of viral shedding from kidney cells rather than of a defect in glomerular filtration. In this regard, a significant and persistent amount of SARS-CoV was detected in the urine of experimentally infected cynomolgus macaques (30). It should be noted that acute renal failure has been reported in SARS cases and that renal tubular epithelial cells represent the main target of the damage. Actually, about 7% of the SARS patients developed acute tubular necrosis with no evidence of glomerular pathology (5). Therefore, our study suggests that virus replication in PTEC might be responsible for, or at least involved in, renal dysfunctions in vivo. Since SARS-CoV infection of tubular epithelial cells did not cause an overt CPE, the possibility of either direct or immune-mediated mechanisms of virus-induced tubular injury should be further investigated. However, it must be taken into account that even minor functional damage of tubular cells has been linked to a negative prognosis in individuals infected with SARS CoV (53).

ACE2 has been identified as the receptor for SARS-CoV in Vero E6 cells (31). ACE2 is abundantly present in humans in the epithelia of lung and small intestine, heart, testis, and also kidney (33). In our study, the distinct susceptibility of the different human renal cells to SARS-CoV infection was in part correlated to differential levels of ACE2 expression. Indeed, despite detectable levels of ACE2 expression on both MC and podocytes, only MC were transiently susceptible, whereas podocytes were clearly nonpermissive to productive SARS-CoV infection. This observation suggests that cofactors or coreceptors other than ACE2 are required in order to confer full susceptibility to productive SARS-CoV infection. In this regard, SARS-CoV has been shown to interact with receptors distinct from ACE2 to gain entry into cells (3). In particular, DC-SIGN (dendritic cell-specific ICAM-grabbing non-integrin) and L-SIGN, both members of the C-type lectin family of receptors, have been shown to serve as SARS-CoV receptors independently of ACE2 (18, 24). We cannot exclude that differential expression of L- or DC-SIGN might influence viral entry in these cells. In addition, factors other than differential expression of ACE2 and L- or DC-SIGN likely play a crucial role in cell susceptibility to SARS-CoV infection, productive virus replication, and cytopathicity. In this regard, Vero E6 cells are known to lack a functional beta interferon (IFN-β)

gene, although the African green monkey-derived MA104 cells are endowed with an intact IFN-β gene and allow replication of SARS-CoV as efficiently as Vero cells (46). In this regard, SARS-CoV has acquired the capacity to curtail the IFN responses (15, 26). Other cellular factors, however, may be involved in protecting PTEC from SARS-CoV CPE, as observed in other in vitro models of viral persistence (10).

In addition to cellular factors, however, mutations in the viral genome occurred during PTEC persistent and productive infection. Culture supernatants generated during each cell division were characterized with regard to potential changes in the virus replication capacity. In this regard, mixed viral populations with different genotypes can coexist in an equilibrium governed by a balance between mutations and general selection. In our case, four serial passages in PTEC were sufficient to select for the fittest variant. By sequencing the entire viral genome, we demonstrated that the nonconservative E11A mutation in the M protein was selected during persistent infection of PTEC and was advantageous for SARS-CoV replication in these cells.

By comparing the sequences available from the Chinese SARS Molecular Epidemiology Consortium, no changes were observed in the M glycoprotein at position 11 (4). However, a variation from glycine (G) to serine (S) was present at position 5 when palm civet sequences were compared to the human sequences collected during the epidemic. Although the role of G5S in viral adaptation and pathogenesis is not yet elucidated, this observation suggests that the M glycoprotein can potentially evolve and play a role during animal-to-human infection. The E11A mutation that evolved during in vitro passages conferred a selective in vitro replication advantage when introduced in the SARS-CoV infectious molecular clone. The consequent size and charge variation produced at the N-terminus ectodomain of the M protein might affect the M function either at the level of viral entry or assembly and budding. In fact, the substitution for a negatively charged amino acid (glutamic acid) with a nonpolar amino acid (alanine) might increase the virus stickiness to the cell membrane, which is usually negatively charged, by the presence of membrane glycosaminoglycans and proteoglycans thus favoring the attachment of the viral particles and engagement of the spike proteins with ACE2. In addition, this mutation could improve the M scaffolding function during virion budding into the lumen of the endoplasmic reticulum (22, 35). Of note is presence of the same amino acid change in the mouse-adapted SARS-CoV 15 (MA15) obtained after 15 serial passages in BALB/c mice (43). The MA15 virus is characterized by a G-to-A substitution at position 26428 that leads to an E11K change in the M protein. This mutation together with five other amino acid changes, of which three are in ORF-1a, one is in ORF-1b, and one is in S, cause disease and mortality in mice (43). The coincidence of the same amino acid change in the M protein following either in vitro or in vivo adaptation suggests that position 11 plays a critical role for viral pathogenesis. In our in vitro model, no changes occurred in the S, nucleocapsid, replicase, or accessory proteins, in support of the observation that a relative higher fixation rate and nonsilent/silent mutation ratio occurred in the M protein compared to the other structural proteins during the epidemic in vivo (50; unpublished observation).

In conclusion, our findings show that human kidney tubular epithelial cells are permissive for productive SARS-CoV infection in vitro, explaining an unexplored but significant aspect of SARS pathogenesis. Further investigation of our in vitro model of SARS-CoV infectivity in different renal cells may provide insights into understanding the mechanisms of kidney injury, resulting in an unfavorable prognosis for many SARS patients. Furthermore, our findings suggest that the kidney, particularly tubular epithelial cells, might be a reservoir of persistent SARS-CoV infection in vivo. The distinct outcome of SARS-CoV infection in cells expressing ACE2 and possibly L- or DC-SIGN could be used to search for host gene expression and/or signaling pathways playing a role in the establishment of SARS-CoV replication and persistence as well as to analyze the selection process underlying viral mutations favoring persistence in human cells.

REFERENCES

1. **Camussi, G., E. Turello, C. Tetta, F. Bussolino, and C. Baglioni.** 1990. Tumor necrosis factor induces contraction of mesangial cells and alters their cytoskeletons. Kidney Int. **38:**795–802.
2. **Chan, P. K., K. F. To, A. W. Lo, J. L. Cheung, I. Chu, F. W. Au, J. H. Tong, J. S. Tam, J. J. Sung, and H. K. Ng.** 2004. Persistent infection of SARS coronavirus in colonic cells in vitro. J. Med. Virol. **74:**1–7.
3. **Chen, J., and K. Subbarao.** 2007. The immunobiology of SARS. Annu. Rev. Immunol. **25:**443–472.
4. **Chinese SARS Molecular Epidemiology Consortium.** 2004. Molecular evolution of the SARS coronavirus during the course of the SARS epidemic in China. Science **303:**1666–1669.
5. **Chu, K. H., W. K. Tsang, C. S. Tang, M. F. Lam, F. M. Lai, K. F. To, K. S. Fung, H. L. Tang, W. W. Yan, H. W. Chan, T. S. Lai, K. L. Tong, and K. N. Lai.** 2005. Acute renal impairment in coronavirus-associated severe acute respiratory syndrome. Kidney Int. **67:**698–705.
6. **Conaldi, P. G., L. Biancone, A. Bottelli, A. De Martino, G. Camussi, and A. Toniolo.** 1997. Distinct pathogenic effects of group B coxsackieviruses on human glomerular and tubular kidney cells. J. Virol. **71:**9180–9187.
7. **Conaldi, P. G., L. Biancone, A. Bottelli, A. Wade-Evans, L. C. Racusen, M. Boccellino, V. Orlandi, C. Serra, G. Camussi, and A. Toniolo.** 1998. HIV-1 kills renal tubular epithelial cells in vitro by triggering an apoptotic pathway involving caspase activation and Fas upregulation. J. Clin. Investig. **102:**2041–2049.
8. **Conaldi, P. G., A. Bottelli, A. Baj, C. Serra, L. Fiore, G. Federico, B. Bussolati, and G. Camussi.** 2002. Human immunodeficiency virus-1 tat induces hyperproliferation and dysregulation of renal glomerular epithelial cells. Am. J. Pathol. **161:**53–61.
9. **Conaldi, P. G., A. Bottelli, A. Wade-Evans, L. Biancone, A. Baj, V. Cantaluppi, C. Serra, A. Dolei, A. Toniolo, and G. Camussi.** 2000. HIV-persistent infection and cytokine induction in mesangial cells: a potential mechanism for HIV-associated glomerulosclerosis. AIDS **14:**2045–2047.
10. **Conaldi, P. G., C. Serra, A. Mossa, V. Falcone, F. Basolo, G. Camussi, A. Dolei, and A. Toniolo.** 1997. Persistent infection of human vascular endothelial cells by group B coxsackieviruses. J. Infect. Dis. **175:**693–696.
11. **Ding, Y., L. He, Q. Zhang, Z. Huang, X. Che, J. Hou, H. Wang, H. Shen, L. Qiu, Z. Li, J. Geng, J. Cai, H. Han, X. Li, W. Kang, D. Weng, P. Liang, and S. Jiang.** 2004. Organ distribution of severe acute respiratory syndrome (SARS) associated coronavirus (SARS-CoV) in SARS patients: implications for pathogenesis and virus transmission pathways. J. Pathol. **203:**622–630.
12. **Drosten, C., S. Gunther, W. Preiser, S. van der Werf, H. R. Brodt, S. Becker, H. Rabenau, M. Panning, L. Kolesnikova, R. A. Fouchier, A. Berger, A. M. Burguiere, J. Cinatl, M. Eickmann, N. Escriou, K. Grywna, S. Kramme, J. C. Manuguerra, S. Muller, V. Rickerts, M. Sturmer, S. Vieth, H. D. Klenk, A. D. Osterhaus, H. Schmitz, and H. W. Doerr.** 2003. Identification of a novel coronavirus in patients with severe acute respiratory syndrome. N. Engl. J. Med. **348:**1967–1976.
13. **Farcas, G. A., S. M. Poutanen, T. Mazzulli, B. M. Willey, J. Butany, S. L. Asa, P. Faure, P. Akhavan, D. E. Low, and K. C. Kain.** 2005. Fatal severe acute respiratory syndrome is associated with multiorgan involvement by coronavirus. J. Infect. Dis. **191:**193–197.
14. **Fouchier, R. A., T. Kuiken, M. Schutten, G. van Amerongen, G. J. van Doornum, B. G. van den Hoogen, M. Peiris, W. Lim, K. Stohr, and A. D. Osterhaus.** 2003. Aetiology: Koch's postulates fulfilled for SARS virus. Nature **423:**240.

15. Frieman, M., M. Heise, and R. Baric. 2008. SARS coronavirus and innate immunity. Virus Res. 133:101–112.

16. Gu, J., E. Gong, B. Zhang, J. Zheng, Z. Gao, Y. Zhong, W. Zou, J. Zhan, S. Wang, Z. Xie, H. Zhuang, B. Wu, H. Zhong, H. Shao, W. Fang, D. Gao, F. Pei, X. Li, Z. He, D. Xu, X. Shi, V. M. Anderson, and A. S. Leong. 2005. Multiple organ infection and the pathogenesis of SARS. J. Exp. Med. 202:415–424.

17. Hamming, I., W. Timens, M. L. Bulthuis, A. T. Lely, G. J. Navis, and H. van Goor. 2004. Tissue distribution of ACE2 protein, the functional receptor for SARS coronavirus. A first step in understanding SARS pathogenesis. J. Pathol. 203:631–637.

18. Han, D. P., M. Lohani, and M. W. Cho. 2007. Specific asparagine-linked glycosylation sites are critical for DC-SIGN- and L-SIGN-mediated severe acute respiratory syndrome coronavirus entry. J. Virol. 81:12029–12039.

19. Holmes, K. V. 2003. SARS coronavirus: a new challenge for prevention and therapy. J. Clin. Investig. 111:1605–1609.

20. Hon, K. L., C. W. Leung, W. T. Cheng, P. K. Chan, W. C. Chu, Y. W. Kwan, A. M. Li, N. C. Fong, P. C. Ng, M. C. Chiu, C. K. Li, J. S. Tam, and T. F. Fok. 2003. Clinical presentations and outcome of severe acute respiratory syndrome in children. Lancet 361:1701–1703.

21. Huang, I. C., B. J. Bosch, F. Li, W. Li, K. H. Lee, S. Ghiran, N. Vasilieva, T. S. Dermody, S. C. Harrison, P. R. Dormitzer, M. Farzan, P. J. Rottier, and H. Choe. 2006. SARS coronavirus, but not human coronavirus NL63, utilizes cathepsin L to infect ACE2-expressing cells. J. Biol. Chem. 281:3198–3203.

22. Huang, Y., Z.-Y. Yang, W.-P. Kong, and G. J. Nabel. 2004. Generation of synthetic severe acute respiratory syndrome coronavirus pseudoparticles: implications for assembly and vaccine production. J. Virol. 78:12557–12565.

23. Hung, I. F., V. C. Cheng, A. K. Wu, B. S. Tang, K. H. Chan, C. M. Chu, M. M. Wong, W. T. Hui, L. L. Poon, D. M. Tse, K. S. Chan, P. C. Woo, S. K. Lau, J. S. Peiris, and K. Y. Yuen. 2004. Viral loads in clinical specimens and SARS manifestations. Emerg. Infect. Dis. 10:1550–1557.

24. Jeffers, S. A., S. M. Tusell, L. Gillim-Ross, E. M. Hemmila, J. E. Achenbach, G. J. Babcock, W. D. Thomas, Jr., L. B. Thackray, M. D. Young, R. J. Mason, D. M. Ambrosino, D. E. Wentworth, J. C. Demartini, and K. V. Holmes. 2004. CD209L (L-SIGN) is a receptor for severe acute respiratory syndrome coronavirus. Proc. Natl. Acad. Sci. USA 101:15748–15753.

25. Kerjaschki, D. 1994. Dysfunctions of cell biological mechanisms of visceral epithelial cell (podocytes) in glomerular diseases. Kidney Int. 45:300–313.

26. Kopecky-Bromberg, S. A., L. Martinez-Sobrido, M. Frieman, R. A. Baric, and P. Palese. 2007. Severe acute respiratory syndrome coronavirus open reading frame (ORF) 3b, ORF 6, and nucleocapsid proteins function as interferon antagonists. J. Virol. 81:548–557.

27. Ksiazek, T. G., D. Erdman, C. S. Goldsmith, S. R. Zaki, T. Peret, S. Emery, S. Tong, C. Urbani, J. A. Comer, W. Lim, P. E. Rollin, S. F. Dowell, A. E. Ling, C. D. Humphrey, W. J. Shieh, J. Guarner, C. D. Paddock, P. Rota, B. Fields, J. DeRisi, J. Y. Yang, N. Cox, J. M. Hughes, J. W. LeDuc, W. J. Bellini, and L. J. Anderson. 2003. A novel coronavirus associated with severe acute respiratory syndrome. N. Engl. J. Med. 348:1953–1966.

28. Kuiken, T., R. A. Fouchier, M. Schutten, G. F. Rimmelzwaan, G. van Amerongen, D. van Riel, J. D. Laman, T. de Jong, G. van Doornum, W. Lim, A. E. Ling, P. K. Chan, J. S. Tam, M. C. Zambon, R. Gopal, C. Drosten, S. van der Werf, N. Escriou, J. C. Manuguerra, K. Stohr, J. S. Peiris, and A. D. Osterhaus. 2003. Newly discovered coronavirus as the primary cause of severe acute respiratory syndrome. Lancet 362:263–270.

29. Lau, Y. L., and J. S. Peiris. 2005. Pathogenesis of severe acute respiratory syndrome. Curr. Opin. Immunol. 17:404–410.

30. Lawler, J. V., T. P. Endy, L. E. Hensley, A. Garrison, E. A. Fritz, M. Lesar, R. S. Baric, D. A. Kulesh, D. A. Norwood, L. P. Wasieloski, M. P. Ulrich, T. R. Slezak, E. Vitalis, J. W. Huggins, P. B. Jahrling, and J. Paragas. 2006. Cynomolgus macaque as an animal model for severe acute respiratory syndrome. PLoS Med. 3:e149.

31. Li, W., M. J. Moore, N. Vasilieva, J. Sui, S. K. Wong, M. A. Berne, M. Somasundaran, J. L. Sullivan, K. Luzuriaga, T. C. Greenough, H. Choe, and M. Farzan. 2003. Angiotensin-converting enzyme 2 is a functional receptor for the SARS coronavirus. Nature 426:450–454.

32. Li, W., Z. Shi, M. Yu, W. Ren, C. Smith, J. H. Epstein, H. Wang, G. Crameri, Z. Hu, H. Zhang, J. Zhang, J. McEachern, H. Field, P. Daszak, B. T. Eaton, S. Zhang, and L. F. Wang. 2005. Bats are natural reservoirs of SARS-like coronaviruses. Science 310:676–679.

33. Li, W., S.-K. Wong, F. Li, J. H. Kuhn, I.-C. Huang, H. Choe, and M. Farzan. 2006. Animal origins of the severe acute respiratory syndrome coronavirus: insight from ACE2–S-protein interactions. J. Virol. 80:4211–4219.

34. Madsen, K. M., and B. M. Brenner. 1989. Structure and function of the renal tubule and interstitium, p. 606–641. In C. O. Tischer and B. M. Brenner (ed.), Renal pathology with clinical and functional correlations. J. B. Lippincott, Philadelphia, PA.

35. McBride, C. E., J. Li, and C. E. Machamer. 2007. The cytoplasmic tail of the severe acute respiratory syndrome coronavirus spike protein contains a novel endoplasmic reticulum retrieval signal that binds COPI and promotes interaction with membrane protein. J. Virol. 81:2418–2428.

36. Mizutani, T., S. Fukushi, M. Saijo, I. Kurane, and S. Morikawa. 2005. JNK

37. Peiris, J. S., C. M. Chu, V. C. Cheng, K. S. Chan, I. F. Hung, L. L. Poon, K. I. Law, B. S. Tang, T. Y. Hon, C. S. Chan, K. H. Chan, J. S. Ng, B. J. Zheng, W. L. Ng, R. W. Lai, Y. Guan, and K. Y. Yuen. 2003. Clinical progression and viral load in a community outbreak of coronavirus-associated SARS pneumonia: a prospective study. Lancet 361:1767–1772.

38. Peiris, J. S., S. T. Lai, L. L. Poon, Y. Guan, L. Y. Yam, W. Lim, J. Nicholls, W. K. Yee, W. W. Yan, M. T. Cheung, V. C. Cheng, K. H. Chan, D. N. Tsang, R. W. Yung, T. K. Ng, and K. Y. Yuen. 2003. Coronavirus as a possible cause of severe acute respiratory syndrome. Lancet 361:1319–1325.

39. Peiris, J. S., K. Y. Yuen, A. D. Osterhaus, and K. Stohr. 2003. The severe acute respiratory syndrome. N. Engl. J. Med. 349:2431–2441.

40. Pinna, D., A. Sampson-Johannes, M. Clementi, G. Poli, S. Rossini, L. Lin, and E. Vicenzi. 2005. Amotosalen photochemical inactivation of severe acute respiratory syndrome coronavirus in human platelet concentrates. Transfus. Med. 15:269–276.

41. Prabakaran, P., X. Xiao, and D. S. Dimitrov. 2004. A model of the ACE2 structure and function as a SARS-CoV receptor. Biochem. Biophys. Res. Commun. 314:235–241.

42. Racusen, L. C., C. Monteil, A. Sgrignoli, M. Lucskay, S. Marouillat, J. G. Rhim, and J. P. Morin. 1997. Cell lines with extended in vitro growth potential from human renal proximal tubule: characterization, response to inducers, and comparison with established cell lines. J. Lab. Clin. Med. 129:318–329.

43. Roberts, A., D. Deming, C. D. Paddock, A. Cheng, B. Yount, L. Vogel, B. D. Herman, T. Sheahan, M. Heise, G. L. Genrich, S. R. Zaki, R. Baric, and K. Subbarao. 2007. A mouse-adapted SARS-coronavirus causes disease and mortality in BALB/c mice. PLoS Pathog. 3:e5.

44. Ruan, Y. J., C. L. Wei, A. L. Ee, V. B. Vega, H. Thoreau, S. T. Su, J. M. Chia, P. Ng, K. P. Chiu, L. Lim, T. Zhang, C. K. Peng, E. O. Lin, N. M. Lee, S. L. Yee, L. F. Ng, R. E. Chee, L. W. Stanton, P. M. Long, and E. T. Liu. 2003. Comparative full-length genome sequence analysis of 14 SARS coronavirus isolates and common mutations associated with putative origins of infection. Lancet 361:1779–1785.

45. Sawicki, S. G., and D. L. Sawicki. 2005. Coronavirus transcription: a perspective. Curr. Top. Microbiol. Immunol. 287:31–55.

46. Sims, A. C., S. E. Burkett, B. Yount, and R. J. Pickles. 2008. SARS-CoV replication and pathogenesis in an in vitro model of the human conducting airway epithelium. Virus Res. 133:33–44.

47. Spaan, W., H. Delius, M. Skinner, J. Armstrong, P. Rottier, S. Smeekens, B. A. van der Zeijst, and S. G. Siddell. 1983. Coronavirus mRNA synthesis involves fusion of non-contiguous sequences. EMBO J. 2:1839–1844.

48. Striker, G. E., and L. J. Striker. 1985. Glomerular cell culture. Lab. Investig. 53:122–131.

49. To, K. F., J. H. Tong, P. K. Chan, F. W. Au, S. S. Chim, K. C. Chan, J. L. Cheung, E. Y. Liu, G. M. Tse, A. W. Lo, Y. M. Lo, and H. K. Ng. 2004. Tissue and cellular tropism of the coronavirus associated with severe acute respiratory syndrome: an in-situ hybridization study of fatal cases. J. Pathol. 202:157–163.

50. Vega, V. B., Y. Ruan, J. Liu, W. H. Lee, C. L. Wei, S. Y. Se-Thoe, K. F. Tang, T. Zhang, P. R. Kolatkar, E. E. Ooi, A. E. Ling, L. W. Stanton, P. M. Long, and E. T. Liu. 2004. Mutational dynamics of the SARS coronavirus in cell culture and human populations isolated in 2003. BMC Infect. Dis. 4:32.

51. Vicenzi, E., F. Canducci, D. Pinna, N. Mancini, S. Carletti, A. Lazzarin, C. Bordignon, G. Poli, and M. Clementi. 2004. Coronaviridae and SARS-associated coronavirus strain HSR1. Emerg. Infect. Dis. 10:413–418.

52. World Health Organization. 2003. Summary of SARS cases with onset of illness from 1 November 2002 to 31 July 2003. World Health Organization, Geneva, Switzerland. http://www.who.int/csr/sars/country/table2004_04_21/en/index.html.

53. Wu, V. C., J. W. Huang, P. R. Hsueh, Y. F. Yang, H. B. Tsai, W. C. Kan, H. W. Chang, and K. D. Wu. 2005. Renal hypouricemia is an ominous sign in patients with severe acute respiratory syndrome. Am. J. Kidney Dis. 45:88–95.

54. Yam, W. C., K. H. Chan, L. L. M. Poon, Y. Guan, K. Y. Yuen, W. H. Seto, and J. S. M. Peiris. 2003. Evaluation of reverse transcription-PCR assays for rapid diagnosis of severe acute respiratory syndrome associated with a novel coronavirus. J. Clin. Microbiol. 41:4521–5424.

55. Yamate, M., M. Yamashita, T. Goto, S. Tsuji, Y. G. Li, J. Warachit, M. Yunoki, and K. Ikuta. 2005. Establishment of Vero E6 cell clones persistently infected with severe acute respiratory syndrome coronavirus. Microbes Infect. 7:1530–1540.

56. Yang, Z.-Y., Y. Huang, L. Ganesh, K. Leung, W.-P. Kong, O. Schwartz, K. Subbarao, and G. J. Nabel. 2004. pH-dependent entry of severe acute respiratory syndrome coronavirus is mediated by the spike glycoprotein and enhanced by dendritic cell transfer through DC-SIGN. J. Virol. 78:5642–5650.

57. Yount, B., K. M. Curtis, E. A. Fritz, L. E. Hensley, P. B. Jahrling, E. Prentice, M. R. Denison, T. W. Geisbert, and R. S. Baric. 2003. Reverse genetics with a full-length infectious cDNA of severe acute respiratory syndrome coronavirus. Proc. Natl. Acad. Sci. USA 100:12995–13000.

and PI3k/Akt signaling pathways are required for establishing persistent SARS-CoV infection in Vero E6 cells. Biochim. Biophys. Acta 1741:4–10.